

Dark spatial solitons in non-Kerr-law media

Yijiang Chen

Optical Sciences Centre, Australian National University, Canberra, Australia

(Received 16 September 1991)

Two-dimensional light trapping of TM and TE patterns in saturable self-defocusing nonlinear media is examined. The vector dark spatial soliton of TM type is found to exist only within a certain range of the beam effective index, which can be wider or narrower compared with the corresponding one in the Kerr-law nonlinearity, depending on the nonlinear saturation index. This contrasts with the scalar dark spatial soliton of TE type, the guidable region of which in saturable nonlinear media is equal to or narrower than that in the Kerr-law nonlinear medium. The physical origin leading to such a distinct contrast is also explored.

PACS number(s): 42.65.-k

Spatial solitons are the stable entity of two-dimensional solitary waves trapped in uniform nonlinear media [1–11]. Similar to temporal solitons, spatial solitons come in two varieties: the bright and the dark. The fundamental bright spatial soliton denotes the two-dimensional stationary self-guided bright beam propagating stably in a self-focusing nonlinear medium above the cutoff of its self-induced index profile [6], while the fundamental dark spatial soliton means the two-dimensional stationary self-guided dark beam evolving stably in a self-defocusing nonlinear medium at the cutoff [11]. In a Kerr-law medium, a dark spatial soliton, like a bright one, can be trapped in the form of TE and TM patterns. But in contrast to its bright counterpart, the existence of the TM dark beam is limited in the range of the beam effective index n_{eff} (defined as the beam propagation constant β divided by the wave number k of free space) from $0.82n_0$ to n_0 the linear refractive index of the medium, whereas that of the dark TE beam extends over all possible values of n_{eff} ranging from 0 to n_0 [11].

The Kerr-law nonlinearity is an idealized model simulating the nonlinearity-induced index change when the beam intensity is not too high. In reality, the nonlinearity induced index change saturates at a certain level. This saturation effect manifests itself significantly especially when high nonlinearity is involved [8–10,12]. Accordingly, there appears a need for exploring the possibility of self-trapping in saturable self-defocusing nonlinear media to see how nonlinear saturation manipulates trapping characteristics of TM and TE patterns and how a TM beam departs significantly from a TE beam.

Propagation of a light wave in a medium is governed by Maxwell's equations [11]

$$\nabla \times \nabla \times \mathbf{E} = k^2 \epsilon(|\mathbf{E}|^2) \mathbf{E} \quad (1)$$

with ϵ the relative permittivity. In a self-defocusing nonlinear medium, ϵ decreases with increasing electric field intensity $|\mathbf{E}|^2$. For a saturable nonlinearity the maximum permittivity change is limited to a certain value. A typical model describing this nonlinear saturation is the exponential saturation $\epsilon = \epsilon_0 - (\epsilon_0 - \epsilon_m) \{1 - \exp[-\epsilon_2 |\mathbf{E}|^2 / (\epsilon_0 - \epsilon_m)]\}$, which reduces to the Kerr-law nonlinearity $\epsilon = \epsilon_0 - \epsilon_2 |\mathbf{E}|^2$ as $\epsilon_m \rightarrow -\infty$. Here $\epsilon_0 = n_0^2$ denotes the linear relative permittivity of the medium, ϵ_m ($< \epsilon_0$) is the minimum value of ϵ in the presence of nonlinearity, and ϵ_2 stands for the nonlinear coefficient. This saturable nonlinearity can also be portrayed by other models such as the two-level model $\epsilon = \epsilon_0 - \epsilon_2 |\mathbf{E}|^2 / [1 + \epsilon_2 |\mathbf{E}|^2 / (\epsilon_0 - \epsilon_m)]$. Since these models give the same qualitative picture of light trapping in saturable self-defocusing nonlinear media, without loss of generality we will employ the exponential model in the following study.

As far as isotropic media are concerned, the stationary solutions to Eq. (1) in planar geometry can be decomposed into two sets. One is referred to as a TE set involving one electric-field component $\mathbf{E} = E_y(x, z) \hat{\mathbf{y}} = e_y(x) \exp(i\beta z) \hat{\mathbf{y}}$, which substituted into Eq. (1) yields its normalized governing equation

$$\psi_y'' + \psi_y - f(\psi_y^2) \psi_y = 0 \quad (2)$$

with $f(\eta) = [1 - \exp(-\eta b^2 / \Delta^2)] \Delta^2 / b^2$, the prime denoting derivative with respect to X , the normalized field ψ_y related to e_y by $\psi_y = e_y \sqrt{\epsilon_2 / \epsilon_0} / b$, $X = kb \sqrt{\epsilon_0} x$, the waveguide height $b = (1 - \beta^2 / k_0^2 \epsilon_0)^{1/2}$, and the saturable index height $\Delta = \sqrt{1 - \epsilon_m / \epsilon_0}$. The other is termed as a TM set which involves two field components $\mathbf{E} = [e_x(x) \hat{\mathbf{x}} + e_z(x) \hat{\mathbf{z}}] \exp(i\beta z)$. They are governed by

$$\psi_x' = \frac{\{2b\psi_x\psi_z' \exp[-(\psi_x^2 + \psi_z^2)\Delta^2/b^2] / (1-b^2)^{1/2} + 1/b^2 - f(\psi_x^2 + \psi_z^2)\} \psi_z b (1-b^2)^{1/2}}{1 - \Delta^2 + (\Delta^2 - 2b^2\psi_x^2) \exp[-(\psi_x^2 + \psi_z^2)b^2/\Delta^2]}, \quad (3a)$$

$$\psi_z' = -b [1 - f(\psi_x^2 + \psi_z^2)] \psi_x / (1-b^2)^{1/2}, \quad (3b)$$

where ψ_x and ψ_z are the normalized fields linked to e_x and e_z by $\psi_x = e_x \sqrt{\epsilon_2/\epsilon_0}/b$ and $\psi_z = -ie_z \sqrt{\epsilon_2/\epsilon_0}/b$. Although two differential equations are involved here, actually only one equation needs to be solved for the fields and other trapping characteristics of the beam. This is because the two field components are related by an invariant of the system. This invariant can readily be derived from Eqs. (3a) and (3b) by integration of a combination of the equations. It has the form of

$$b^2\psi_x^2[1-f(\psi_x^2+\psi_z^2)]^2/(1-b^2)+\psi_z^2/b^2 + \psi_x^2 - [\psi_x^2 + \psi_z^2 - f(\psi_x^2 + \psi_z^2)]\Delta^2/b^2 = \Gamma. \quad (4)$$

Accordingly, the solutions to Eq. (3) can then be expressed analytically in an integral form via Eq. (3b)

$$X = -[(1-b^2)^{1/2}/b] \int_{\psi_z(0)}^{\psi_z(X)} d\psi_z / [1-f(\psi_x^2 + \psi_z^2)]\psi_x, \quad (5)$$

where $\psi_x = \psi_x(\psi_z)$ following Eq. (4). The solutions may be solitary, periodic, or growing, depending on the invariant Γ . The characteristic of the solutions may as well be revealed at a glance from the phase space as shown in Fig. 1. Each trajectory in the figure pertains to a particular value of Γ . Enclosed curves are associated with periodic solutions and open trajectories correspond to growing solutions. The solitary waves are identified by the separatrix passing through the equilibrium points $(\psi_x, \psi_z) = (\pm\psi_e, 0)$ (where $\psi'_x = \psi'_z = 0$). The trajectory of this kind only appears in Figs. 1(a) and 1(d) for those marked with arrows. On the contrary, the separatrix marked with arrows which runs through singularities $(\psi_x, \psi_z) = (\pm\psi_s, 0)$ (where $d\psi_x/d\psi_z = 0/0$) appearing in

Fig. 1(b) is associated with the periodic solution. This is because the motion at the singular points does not come to a rest as $\psi'_x \neq 0$ or $\psi'_z \neq 0$, but that at the equilibrium points it does.

The trajectory characteristics illustrated in Fig. 1 cover all the possible values of the waveguide height b and the saturable index height Δ for TM wave solutions. It experiences a qualitative change as the parameters vary. The solitary wave is defined as the solution which satisfies $\psi_x \rightarrow \text{const}$ and $\psi_z \rightarrow \text{const}$ as $X \rightarrow \pm\infty$ and is thus associated only with the separatrix running through the equilibria that occurs in Figs. 1(a) and 1(d). This means that the TM self-guided dark beam can exist only within a certain range of b for a fixed Δ , and its existence can be determined from an examination of the characteristic of the equilibria. The equilibria of the system are defined as a set of values (ψ_x, ψ_z) at which $\psi'_z = \psi'_x = 0$. Equilibria are of two kinds. One is called the elliptical point, which is an isolated point on the phase space surrounded by enclosed curves; at this fixed point, the motion, or ψ_x and ψ_z , remains unchanged as X varies. The other is called the saddle point, which is run through by the separatrix and from which or at which the evolution of a solitary wave starts or terminates at $X = \mp\infty$. The system of Eq. (4) possesses three equilibrium points $(\psi_x, \psi_z) = (0, 0)$ and $(\pm\psi_e, 0)$ with $\psi_e = (\Delta/b)[-\ln(1-b^2/\Delta^2)]^{1/2}$. The point $(0, 0)$ is a fixed point or an elliptical point. But the points $(\pm\psi_e, 0)$ can be elliptical or saddle, subject to the magnitude of b and Δ . This is due to the presence of the singularities which are defined as a set of values (ψ_x, ψ_z) at which $d\psi_x/d\psi_z = 0/0$ (but $\psi'_x \neq 0$ or $\psi'_z \neq 0$). Apparently, an equilibrium must be a singu-

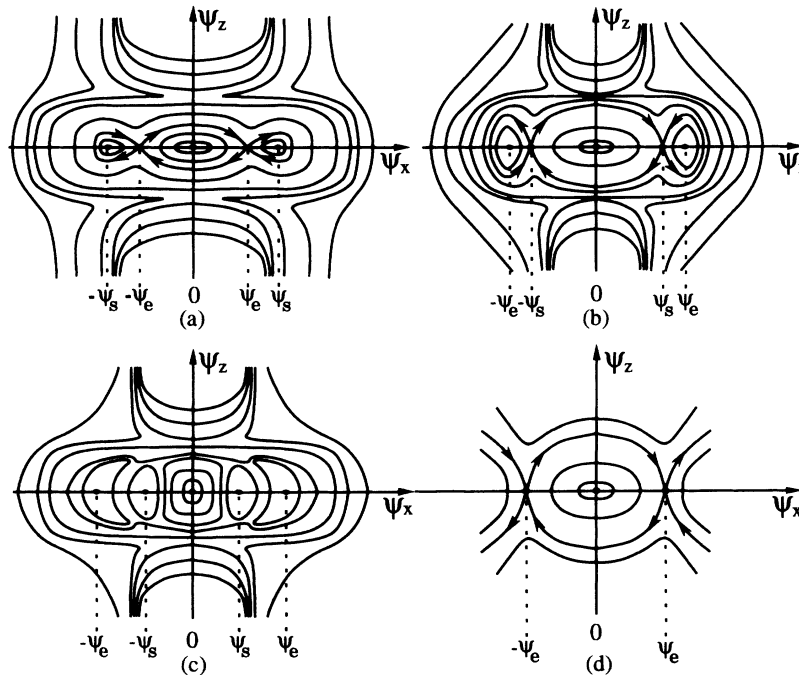


FIG. 1. Characteristics of the trajectories of the TM dark beam on the phase space for (a) $\Delta \geq \Delta_c = 0.83$ and $0 < b < b_c < \Delta$, (b) $\Delta \geq \Delta_c$ and $b_c < b < b_s < \Delta$ (where for the Kerr nonlinearity $b_s = 0.82$), (c) $\Delta < \Delta_c$ and $b_s < b < \min\{1, \Delta\}$, and (d) $\Delta < \Delta_c$ and $0 < b < \Delta$. The relation between b_c and the saturation index Δ is given in Fig. 3(a).

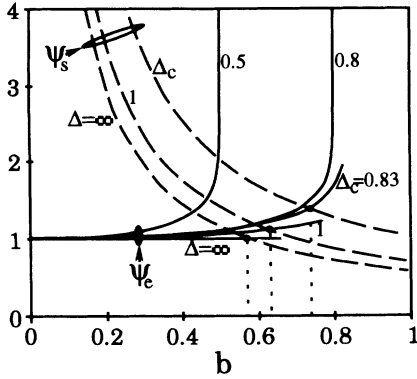


FIG. 2. Dependence of ψ_e and ψ_s on b . $\psi_e = \psi_s$ gives the critical waveguide height b_c below which (i.e., $b < b_c$ corresponding to $\psi_e < \psi_s$) the TM beam is guided.

larity, but the converse is not necessarily so. There possibly exist two singular points for the system of Eq. (3). They are $(\psi_x, \psi_z) = (\pm\psi_s, 0)$ with ψ_s being the root of

$$(1/\Delta^2 - 1)\exp(b^2\psi_s^2/\Delta^2) = (2b^2\psi_s^2/\Delta^2 - 1). \quad (6)$$

When $\psi_e < \psi_s$, the equilibria $(\pm\psi_e, 0)$ are of saddle nature. The set of invariants of Eq. (4) mapped onto the phase space in this case leads to trajectory trait of Fig. 1(a). On the other hand, when $\psi_e > \psi_s$ $(\pm\psi_e, 0)$ become elliptical points. Equation (4) mapped onto the ψ_x - ψ_z plane then gives rise to the trajectory attribute of Fig. 1(b) or 1(c), depending on the value of b and Δ . This indicates the nonexistence of the solitary wave of TM type when $\psi_e > \psi_s$. It follows that $\psi_e = \psi_s$ is the very condition demarcating the existence or nonexistence of the dark solitary wave of TM type. Figure 2 illustrates the dependence of ψ_e and ψ_s on the waveguide height b . As shown, the guidable region $0 < b < b_c$ (with b_c the critical value of b at which $\psi_s = \psi_e$) increases from $b_c = 1/\sqrt{3} \approx 0.58$ for the Kerr-law nonlinearity of $\Delta = \infty$ to $b_c = [(1 - e^{-1.5})/(1 + 2e^{-1.5})]^{1/2} \approx 0.73$ when Δ reduces to $\Delta_c = (1 + 2e^{-1.5})^{-1/2} \approx 0.83$. Thereafter, it decreases with decreasing Δ . This is because the singularities cease to exist below $\Delta = \Delta_c$ as Eq. (6) no longer ad-

mits any root below this value. The guidable region for b is then decided by $0 < b < b_c = \Delta$, limited by the presence of the equilibria $(\pm\psi_e, 0)$ only. [The set of invariants of Eq. (4) mapped onto the phase space in this case gives the trajectory characteristic of Fig. 1(d).] This upper limit b_c of b for self-guidance can actually be derived directly by specifying $\psi_s = \psi_e$ in Eq. (6). This leads to

$$-2(1 - b_c^2/\Delta^2)\ln(1 - b_c^2/\Delta^2) = (1 - b_c^2)/\Delta^2. \quad (7)$$

In the extreme case of $\Delta = \infty$ for the Kerr nonlinearity, the equation reduces to $b_c = 1/\sqrt{3} \approx 0.58$. The solution of b_c to Eq. (7) for a finite Δ can be found by simple geometric analysis which shows that the equation ceases to produce any root when $\Delta < \Delta_c$. In terms of the effective index $n_{\text{eff}} = \beta/k = n_0(1 - b^2)^{1/2}$, the guidable region for the dark spatial TM soliton is shown in Fig. 3(a). Similar to b , the guidable region n_m $[= n_0(1 - b^2)^{1/2}] < n_{\text{eff}} < n_0$ expands from $[0.82n_0, n_0]$ for the Kerr nonlinearity to $[0.68n_0, n_0]$ as Δ reduces from infinity to Δ_c . The guidable region $[n_m, n_0]$ then shrinks with decreasing saturable index height Δ until n_m reaches n_0 as Δ approaches 0.

Extended to Eq. (2), the above analysis then reveals the guiding characteristic of the TE beam. The integration of Eq. (2) upon being multiplied by ψ'_y yields the invariant

$$(\psi'_y)^2 + \psi_y^2 - [\psi_y^2 - f(\psi_y^2)]\Delta^2/b^2 = \Gamma, \quad (8)$$

which gives rise to the solution of the TE beam in an integral form:

$$X = \pm \int_{\psi_y(0)}^{\psi_y(X)} d\psi_y / \{\Gamma - \psi_y^2 + [\psi_y^2 - f(\psi_y^2)]\Delta^2/b^2\}^{1/2}. \quad (9)$$

Mapping the invariant of Eq. (8) onto the phase space consisting of two orthogonal coordinates ψ_y and ψ'_y leads to the trajectory feature of Fig. 1(d), provided that ψ_x and ψ_z there are replaced by ψ_y and ψ'_y . This indicates that the TE-type dark spatial soliton can exist in a saturable nonlinear medium in the range $0 < b < \Delta$ when $\Delta \leq 1$ and $0 < b < 1$ when $\Delta > 1$ or $n_0(1 - \Delta^2)^{1/2} < n_{\text{eff}} < n_0$ when

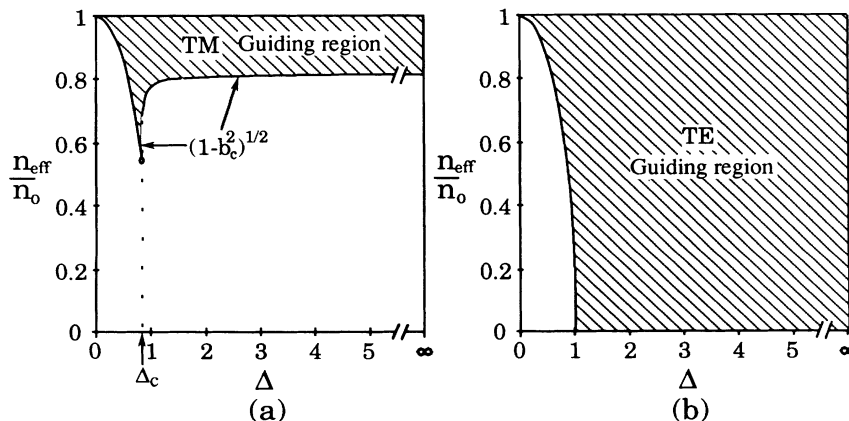


FIG. 3. Guidable regions (shaded) of (a) the TM dark beam and (b) the TE dark beam vs the saturation index Δ where $n_{\text{eff}} = \beta/k$.

$\Delta \leq 1$ and $0 < n_{\text{eff}} < n_0$ when $\Delta > 1$ in terms of the effective wave index. This is shown graphically in Fig. 3(b).

The simple analytic analysis conducted so far explicitly demonstrates the relation between the range of existence of the dark spatial solitons and the saturation parameter. This is confirmed by numerical simulations on Eqs. (2) and (3). However, the detailed knowledge on the field or intensity profiles still requires numerical integral of Eq. (5) or (9). Figure 4 shows the normalized field profiles of the TM and TE beams for various b and Δ . In both cases, the transverse component (ψ_x^2 for TM and ψ_y^2 for TE) exhibits the concave (or dark) intensity profile and the background intensity for both TM and TE beams augments with increasing b at the same rate for a finite Δ [i.e., $\max\{\psi_x^2\} = \max\{\psi_y^2\} = \psi_e^2 = -(\Delta/b)^2 \ln(1 - b^2/\Delta^2)$, which approaches infinity as $b \rightarrow \Delta$], although their profiles differ. This is in contrast to the Kerr-law case [11] for which the normalized background intensity is equal to the constant of unity. As for the beamwidth, it expands with increasing b and the expansion is significant when $b \rightarrow \Delta$, as shown in Fig. 4.

The interesting aspect of the TM dark spatial soliton (absent in the TE case) here is its longitudinal component which displays a bright-field profile. It gradually manifests itself with increasing b , but is almost independent of Δ . It is due to the presence of this longitudinal component that leads to the distinct contrast in self-guidance between TM and TE dark beams. This is because the presence of the longitudinal component tends to exaggerate defocusing thus lessening the self-guidance. This defocusing effect of ψ_z component becomes significant when b is large, as shown in Fig. 5, illustrating the self-induced index profiles, corresponding to the field profiles of Fig. 4. Here, the bright-intensity profile induces an extra hole-index profile which inclines to counterbalance

the convex-index profile created by the dark-intensity profile of the transverse component and thus belittles the self-focusing induced by the transverse component. See, for example, Figs. 4(a) and 5(a) where the refractive index induced by the transverse component ψ_x^2 is indistinguishable from that of the TE beam delineated by the dotted curve, but the total induced index including the contribution from the longitudinal component is weakened compared with n_x^2 . This defocusing effect is strengthened with increasing b as the intensity of the bright longitudinal component increases with increasing b . Therefore, on the one hand, the bright-field distribution of the longitudinal component gradually manifests itself with increasing b , as indicated in Fig. 4, and hence poses a growing demand for the induced index to support. On the other hand, the self-guidance building on the induced index profile is attenuated with increasing b (as illustrated in Fig. 5 or in the relation between $\psi_z^2(0)$ and the peak induced index change $\Delta n_{\text{TM}}^2 = (n_0^2 - n_{\text{eff}}^2)[1 - \psi_z^2(0)] = \Delta n_{\text{TE}}^2 [1 - \psi_z^2(0)]$, which decreases with increasing $\psi_z^2(0)$ and thus with increasing b). Apparently, when b augments to a certain extent exceeding the critical value b_c for $\Delta > \Delta_c$, the longitudinal component becomes so intense and the induced refractive index is so weakened that it can no longer bear the strongly guided bright longitudinal component. Consequently, the self-guidance becomes impossible. However, when Δ is small limited to $\Delta < \Delta_c$, the effect of the longitudinal component become less pronounced since the waveguide height b is limited to small values $b < \Delta < \Delta_c$. Its role in the induced refractive index is then negligible or swamped by the transverse component, which manifests itself dramatically particularly when b is close to Δ . Then the TM beam behaves like the TE beam and the guidable region is decided by $0 < b < \Delta$ as in the TE case. This explains why the guid-

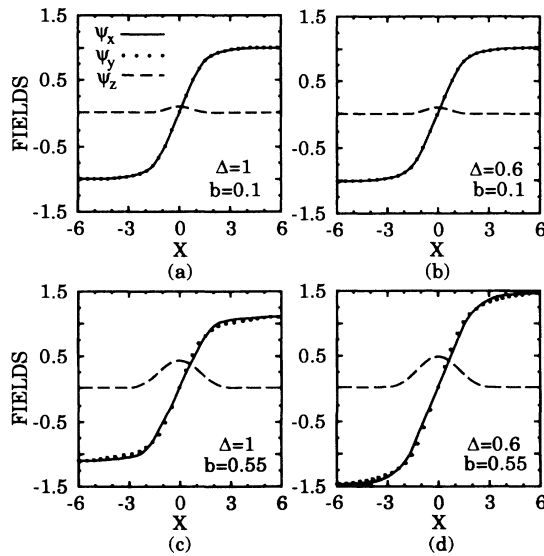


FIG. 4. Field profiles of the dark spatial solitary waves of TM type (the solid curves for ψ_x and the dashed curves for ψ_z) and of TE type (the dotted curves) for different waveguide heights b and saturation indices Δ .

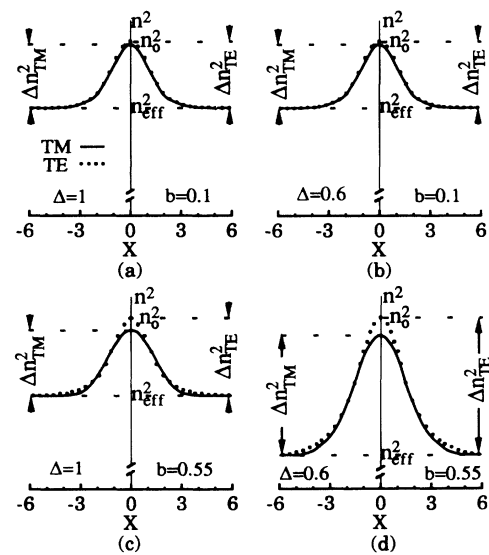


FIG. 5. Induced index profiles $\epsilon = n^2$ corresponding to the field profiles in Fig. 4 where the solid curves are for the TM wave and the dotted curves for the TE wave.

able region for the TM beam can extend to $b = b_c = \Delta$ when $\Delta < \Delta_c$ but $b_c < \Delta$ when $\Delta > \Delta_c$.

Finally, note that as in the case of the Kerr-law nonlinearity, both TM and TE dark beams in saturable nonlinear media operate at the cutoff. The wave effective index $n_{\text{eff}} = \beta/k$, as shown in Fig. 5, equals the minimum value of the induced index profile, irrespective of the magnitudes of b and Δ .

In summary, the phase-space analysis is applied to investigate the dark spatial soliton of TM and TE types in

saturable self-defocusing nonlinear media. The vector dark spatial soliton of TM type is found to exist only within a certain range of the beam effective index, which can be wider or narrower than that in the Kerr-law medium, relying on nonlinear saturation index. This contrasts with the dark spatial soliton of TE type, the guidable region of which in saturable nonlinear media is equal to or narrower than the corresponding one in Kerr-law nonlinearity. The physical origin is also given in accounting for the distinct contrast between TM and TE dark beams.

-
- [1] V. E. Zakharov and A. B. Shabat, *Zh. Eksp. Teor. Fiz.* **61**, 118 (1971) [*Sov. Phys.—JETP* **34**, 62 (1972)].
- [2] A. Barthlemy, S. Maneuf, and C. Froehly, *Opt. Commun.* **55**, 193 (1985).
- [3] S. Maneuf, R. Desailly, and C. Froehly, *Opt. Commun.* **65**, 193 (1988).
- [4] S. Maneuf and F. Reyneud, *Opt. Commun.* **66**, 325 (1988).
- [5] J. S. Aitchison, A. M. Weiner, Y. Silberberg, M. K. Oliver, J. L. Jackel, D. E. Leaird, E. M. Vogel, and P. W. E. Smith, *Opt. Lett.* **15**, 471 (1990).
- [6] Y. Chen, *Electron. Lett.* **27**, 380 (1991).
- [7] V. E. Zakharov and A. B. Shabat, *Zh. Eksp. Teor. Fiz.* **64**, 1627 (1973) [*Sov. Phys.—JETP* **37**, 823 (1973)].
- [8] D. R. Andersen, D. E. Hooton, G. A. Swartzlander, and A. E. Kaplan, *Opt. Lett.* **15**, 783 (1990).
- [9] G. R. Llan, S. R. Skinner, D. R. Andersen, and A. L. Smirl, *Opt. Lett.* **16**, 156 (1991).
- [10] G. A. Swartzlander, D. R. Anderson, J. J. Regan, H. Yin, and A. E. Kaplan, *Phys. Rev. Lett.* **66**, 1583 (1991).
- [11] Y. Chen, *Electron. Lett.* **27**, 1346 (1991).
- [12] M. A. Kramer, W. R. Tompkin, and R. W. Boyd, *Phys. Rev. A* **34**, 2026 (1986).